Electronic Supplementary Material (ESI) for ChemComm.
This journal is © The Royal Society of Chemistry 2020

A New Spin Crossover Fe^{II} Coordination Environment in a Two-Fold Interpenetrated 3-D Hofmann-type Framework Material

Manan Ahmed,[a] Zixi Xie,[b] Shannon Thoonen,[c] Carol Hua,[c] Cameron J. Kepert,[b] Jason R. Price[a,d] and Suzanne M. Neville*[a]

[a.] *School of Chemistry, The University of New South Wales, Sydney, 2052 Australia. *Email: s.neville@unsw.edu.au*
[b.] *The School of Chemistry, The University of Sydney, Sydney, 2006 Australia*
[c.] *School of Chemistry, The University of Melbourne, Parkville, Victoria 3010, Australia.*
[d.] *Australian Synchrotron, ANSTO Clayton, Victoria 3800, Australia*

Supporting information

S1. Experimental

S2. Thermogravimetric analysis

S3. Powder X-ray diffraction

S4. Single crystal X-ray diffraction

S5. Magnetic susceptibility measurements

S6. Raman spectroscopy

S7. References

S1. Experimental

Synthesis of *N1,N3,N5*-tri(pyridin-4-yl)benzene-1,3,5-tricarboxamide (Tbenpy)

The ligand was prepared using the previously reported method with the modification.[1] 1,3,5-benzene tricarbonyl trichloride 1.3584 g (5.133 mmol) was dissolved in 60 mL of THF and 2.70 mL (19.35 mmol) of triethylamine was slowly added in an ice bath at 0 °C. Three equivalent of 4-aminopyridine (1.5796 g, 16.78 mmol) was added to the solution and stirred for 2 h. The temperature was allowed slowly rise to room temperature and then refluxed for two days. The white principate formed was collected by filtration and washed with excess THF and water. The product was purified by stirring 30 min in 1:3 DMSO and water solution. The off-white powder was collected by filtration, washed with an excess of acetone, and dried in an oven for 24 hrs at 60 °C (Yield 2.07 g, 91.5%). ^{1}HNMR (400 MHz, DMSO-d_6, ppm) δ= 10.95 (s, 3H), 8.71-8.76 (m, 3H), 8.50-8.53 (m, 6H), 7.80-7.83 (m, 6H). FTIR (cm^{-1}) 1675(m), 1590(vs), 1499(vs), 1414(w), 1382(vw), 1327(m), 1292(m), 1232(m), 1193(w), 949(vw), 822(m), 708(w), 578(vw), 526(w). Elemental Analysis calc. for $C_{24}H_{18}N_6O_3$ (%): C 65.75; H 4.14; N 19.17; found: C 64.34, H 4.22, N 19.93.

Synthesis of $[Fe_2(Tbenpy)_2(Au(CN)_2)_4]\cdot\{2H_2O,DMF\}$

Single crystals were obtained through the vial-in-vial slow diffusion technique. A mixture of $K_2[Au(CN)_2]$ (23 mg, 0.08 mmol) and Tbenpy (35.08 mg, 0.08 mmol) was placed in the large vial and $Fe(ClO_4)_2\cdot 6H_2O$ 15.1 mg (0.06 mmol) was placed in the small vial. A small vial was then inserted into the large vial and filled carefully with ethanol and large vial carefully filled with 1 mL DMF and ethanol to allow slow diffusion. Square shaped yellow single crystals were formed around the small vial over 10 weeks (Yield: 60.1%). Elemental Analysis calc. for $Fe_2Au_4C_{62}H_{58}N_{22}O_{12}$ (%): C 33.77; H 2.63; N 13.98. Found (%): C 33.46; H 2.37; N 12.80. FT-IR bands (cm^{-1}): 2160(m), 1685(vw), 1654(m), 1590(vs), 1508(vs), 1420(w), 1386(vw), 1329(m), 1291(w), 1230(w), 1209(s), 1094(w), 1044(w), 1014(m), 827(s), 723(w), 662(w), 591(w), 534(s).

Materials and physical measurements

All chemicals were purchased commercially from Sigma Aldrich, Alfa Aesar, Chem-supply and Acros chemical and used without further purification. Fourier transformation (FTIR) was performed on a Thermo-Fisher Nicolet-iS5 spectrometer equipped with a smart iD7 diamond attenuated total reflectance (ATR) windows. The data were collected using the 8 cm^{-1} resolution and 16 scans over the range of 400-4000 cm^{-1}. ^{1}H NMR was conducted on Bruker 400 MHz NMR spectrometer, equipped with an autosampler. Chemical shifts are reported in ppm with the internal TMS signal at 0 ppm as a standard. Elemental analysis was performed at Mark Wainwright analytical centre, UNSW, and at The Campbell Microanalytical Laboratory, University of Otago. Thermogravimetric analysis (TGA) was performed on a Mettler TGA/SDTA851 instrument using 8.5 mg of the sample from 30−600 °C using an aluminium pan and heated at a rate of 1 °C/min under a nitrogen atmosphere.

Magnetic measurement

Temperature-dependent magnetic susceptibility measurements were performed on Quantum Design Versalab magnetometer with a vibrating sample mount (VSM) attachment. The crystalline samples were retained in the mother liquor and sealed with a Teflon tape in the polyethylene tube specially design for measurement. A field of 0.3 T was applied over the temperature range of 300-50-300 K with a scan rate of 0.5, 4, 1 and 2 K min^{-1}.

Single crystal X-ray diffraction

A yellow square-shaped single crystal was mounted in a cryoloop with paratone-N oil. Data collection was carried out on the MX2 beamline at the Australian Synchrotron.[2] Diffraction data were collected using EIGER X 16M detector and Si⟨111⟩ monochromated synchrotron X-ray radiation (λ=0.71073 Å). The crystal was positioned at 110 mm from the detector and the spots were measured using 2s exposure time using the BlueIce software.[3] The data were auto processed on the MX2 beamline using the XDS software.[4] An Oxford cryo-stream controller was used to acquire the data collection in all case to control the temperature. Data were collected at 10 K increments over the 250-100 K temperature range.

The data processing was carried out within *XPREP*[5] and all structures were solved using *ShelXT* [6] and refined on F^2 by full-matrix least-square with *ShelXL*[7] within the X-Seed 4000 or Olex2 program interfaces.[8, 9] All non-hydrogen atoms were refined with anisotropic thermal parameters. Hydrogen atoms were placed at idealized positions and refined using the riding model. Details of the crystallographic data collection and refinement parameters are summarised in Table S1 and selected parameters in Table S2.

CCDC 2042801-2042816 for 100, 110, 120, 130, 140, 150, 160, 170, 180, 190, 200, 210, 220, 230, 240, 250 K, respectively.

Powder X-ray diffraction

Variable temperature X-ray powder diffraction data were collected at the Powder Diffraction beamline BL-10 (20.99 keV and 0.5903 Å) at the Australian Synchrotron.[10] A polycrystalline sample was ground gently into a slurry using a mortar and pestle, packed into borosilicate glass capillary tube of 0.7 mm diameter, and mounted onto the powder diffraction beamline. The capillary was rotated at 1Hz during data collection to aide powder averaging. The beamline was set up with a nominal wavelength of 1.0 Å; the wavelength was determined accurately using NIST SRM LaB6 660b standard. Temperature-dependent data were then collected upon cooling from 90 to 250 K. Data were collected using the Mythen microstrip detector[11] from 1.5 to 75° in 2θ. To cover the gaps between detector modules, two data sets, each of 60 seconds in duration, were collected with the detector set 5° apart and these were then merged to give a single data set using in-house software PDViPER. A slit size of 2 mm was used, to ensure that the fraction of the capillary illuminated by the X-ray beam is the same as the isothermal zone on the cryostream. Le-Bail analysis and peak fitting were performed using TOPAS software package.[12]

Variable temperature Raman spectroscopy

Raman spectra were collected on a Renishaw in Via-Qontor Upright microscope. The excitation wavelength of 785 nm (10 or 50% laser power through a L× 50 objective) was used to acquire the Raman spectra in the range of 150-2300 cm^{-1} with a 10s exposure time. Sample was mounted on the Linkam-FTIR 600 variable temperature stage. Liquid nitrogen was continuously flowed onto the Linkam stage with temperature programmer and cooling pump connected. Prior to measurement, the sample was loaded into a 0.5 mm glass capillary and flame-sealed. Data were collected over the range 250 – 150 K at 10 K steps. Note: data were collected 150 – 100 K but the frozen solvent in the capillary prevented interpretation of these data.

S2. Thermogravimetric analysis

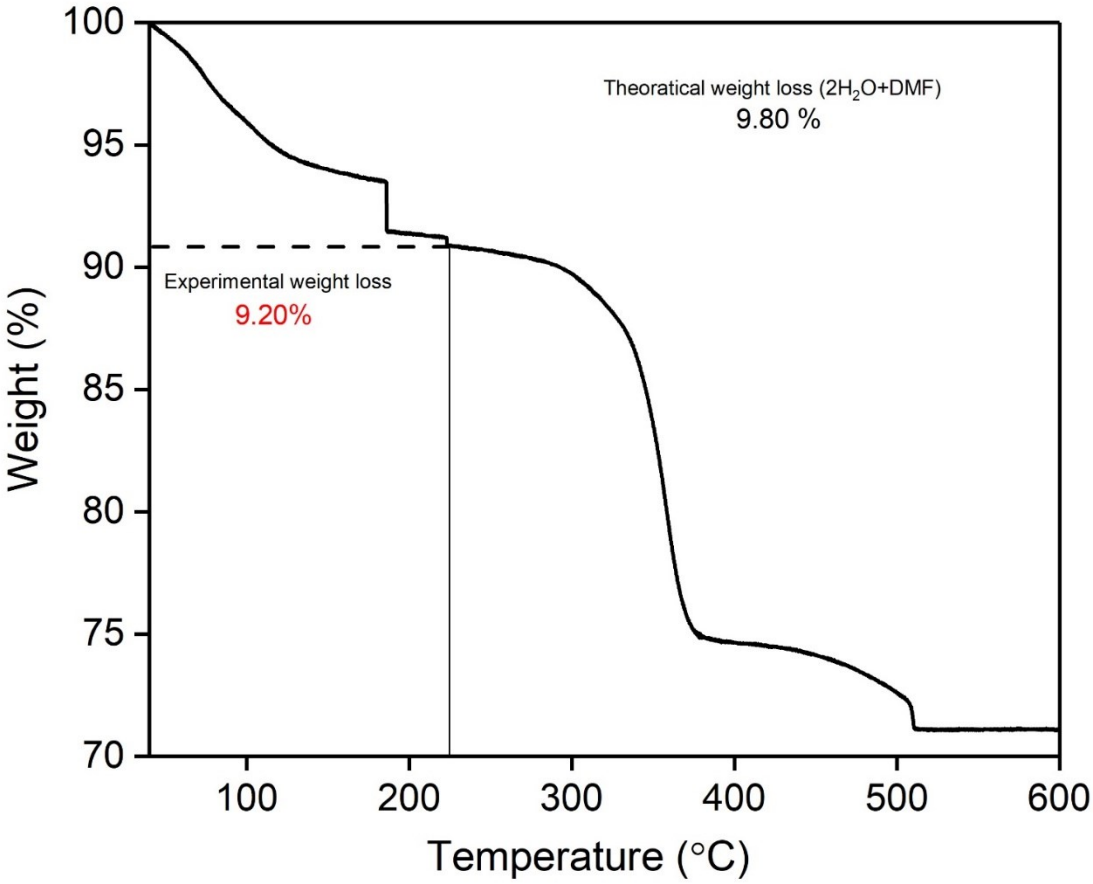

Figure S1. Thermogravimetric analysis of $[Fe^{II}(Tbenpy)(Au(CN)_2)_2]\cdot\{2H_2O,DMF\}$ showing the solvent loss in two steps with an overall loss of ~9.2% (*cf.* theoretical 9.80 %) up to 220 °C.

S3. Powder X-ray diffraction

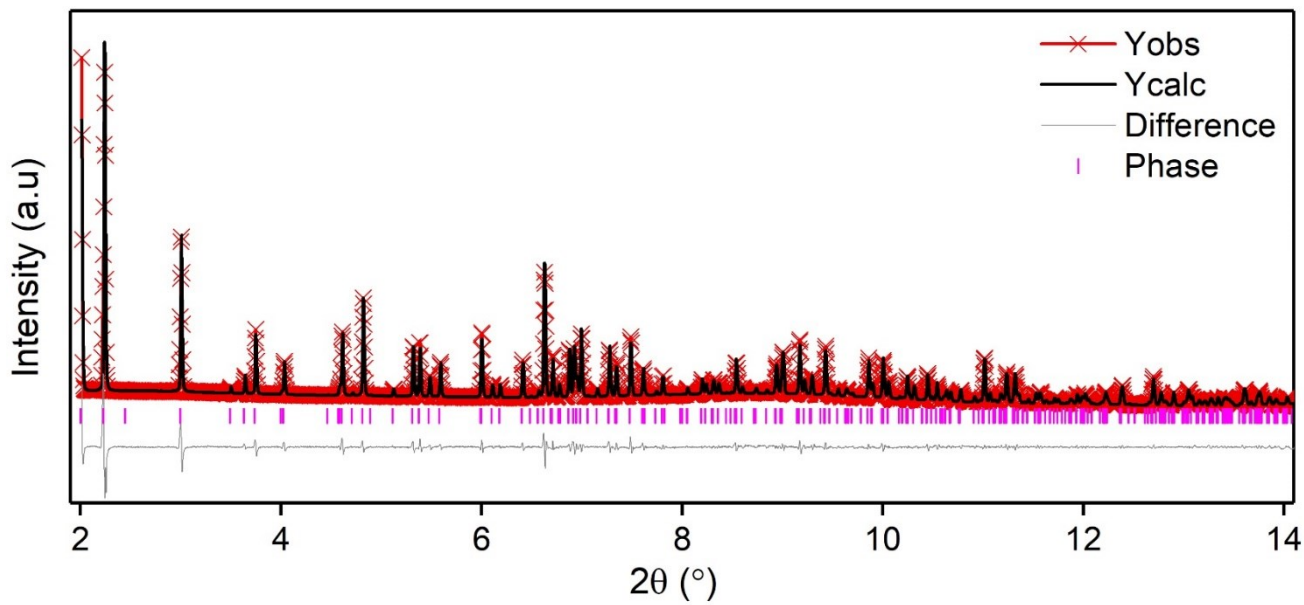

Figure S2. Powder diffraction Le Bail refinement of $[Fe^{II}(Tbenpy)(Au(CN)_2)_2]\cdot\{2H_2O,DMF\}$ at 250 K. Refined parameters: a = 10.502 Å, b = 30.638 Å and c = 34.226 Å, V = 11013.60 Å^3 (*cf.* single crystal at 250 K: a = 10.472 , b = 30.641, c = 34.155, V = 10959 Å^3).

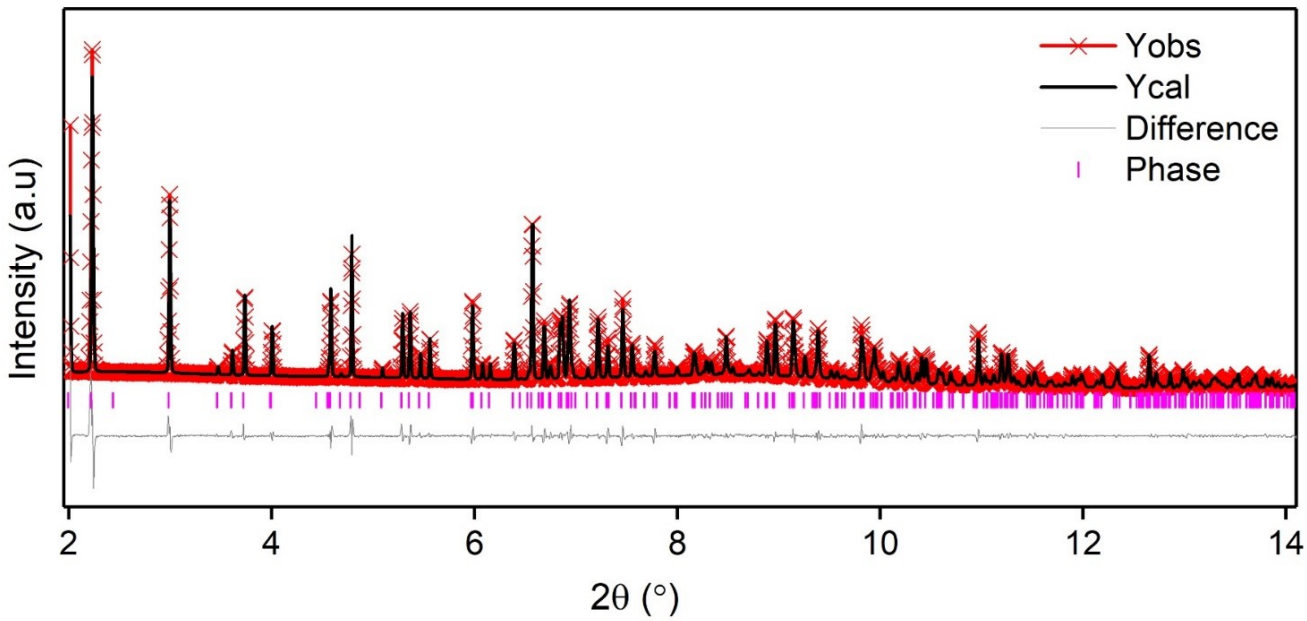

Figure S3. Powder diffraction Le Bail refinement of $[Fe^{II}(Tbenpy)(Au(CN)_2)_2]\cdot\{2H_2O,DMF\}$ at 150 K. Refined parameters: a = 10.301 Å, b = 30.431 Å and c = 33.892 Å, V = 10624.59 Å^3 (*cf.* single crystal at 250 K: a = 10.121 , b = 30.275, c = 33.568, V = 10286 Å^3).

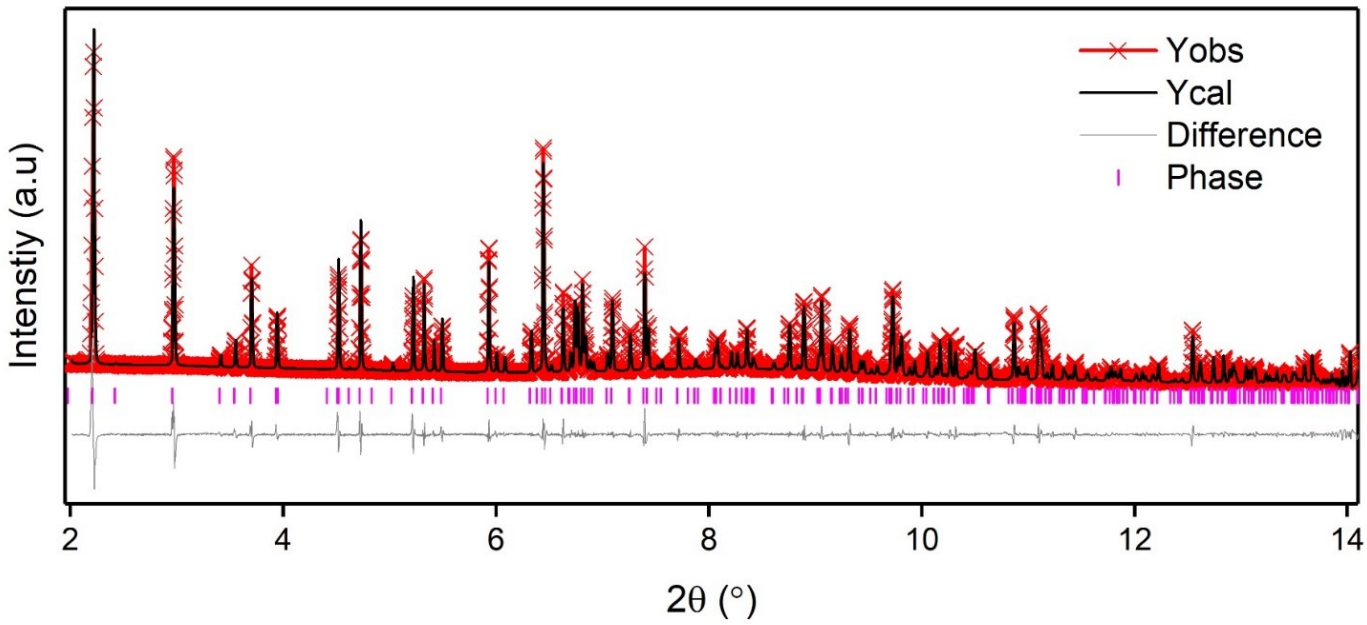

Figure S4. Powder diffraction Le Bail refinement of $[Fe(Tbenpy)(Au(CN)_2)_2]\cdot\{2H_2O,DMF\}$ at 100 K. Refined parameters: a = 10.208 Å, b = 30.287 Å and c = 33.780 Å, V = 10446.05 Å^3 (*cf.* single crystal at 250 K: a = 10.095 , b = 30.238, c = 33.510, V = 10229 Å^3).

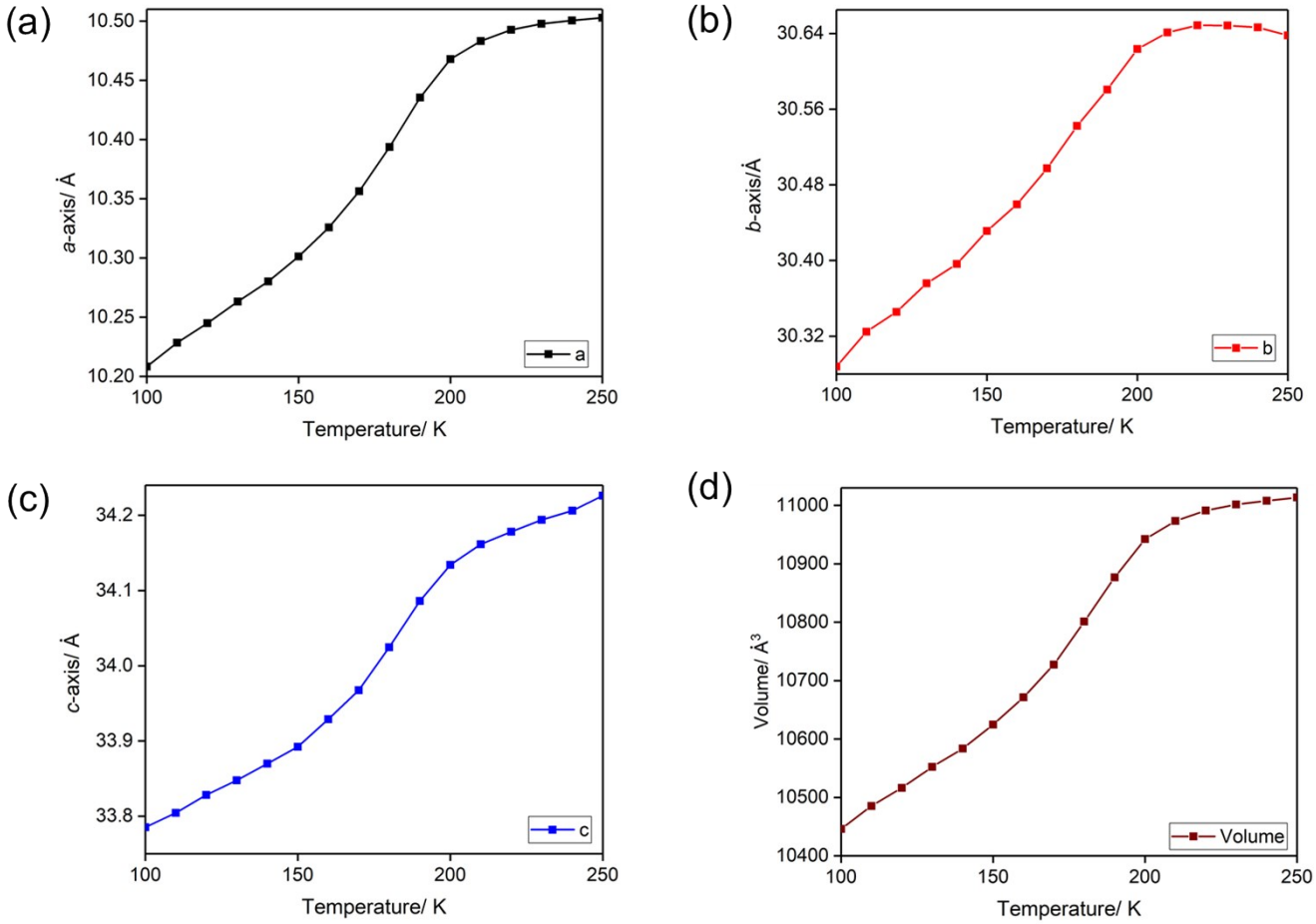

Figure S5. Powder diffraction (a) *a*-axis, (b) *b*-axis, (c) *c*-axis and (d) unit cell volume evolution versus temperature (90 -250 K) for $[Fe^{II}(Tbenpy)(Au(CN)_2)_2]\cdot\{2H_2O,DMF\}$.

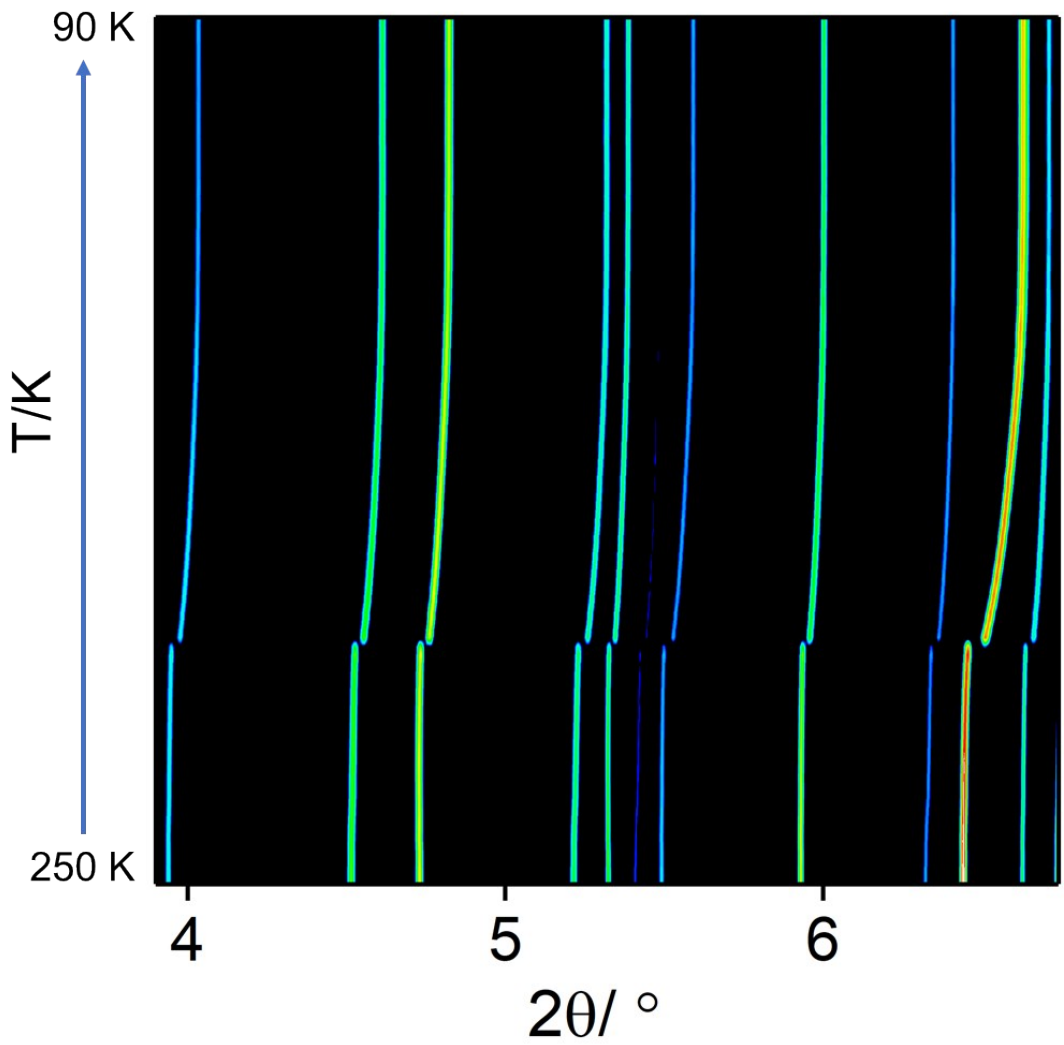

Figure S6. Variable temperature powder diffraction peak evolution of [Fe^{II}(Tbenpy)($Au(CN)_2$)$_2$]·{2 H_2O, DMF} over the temperature range 90–250 K.

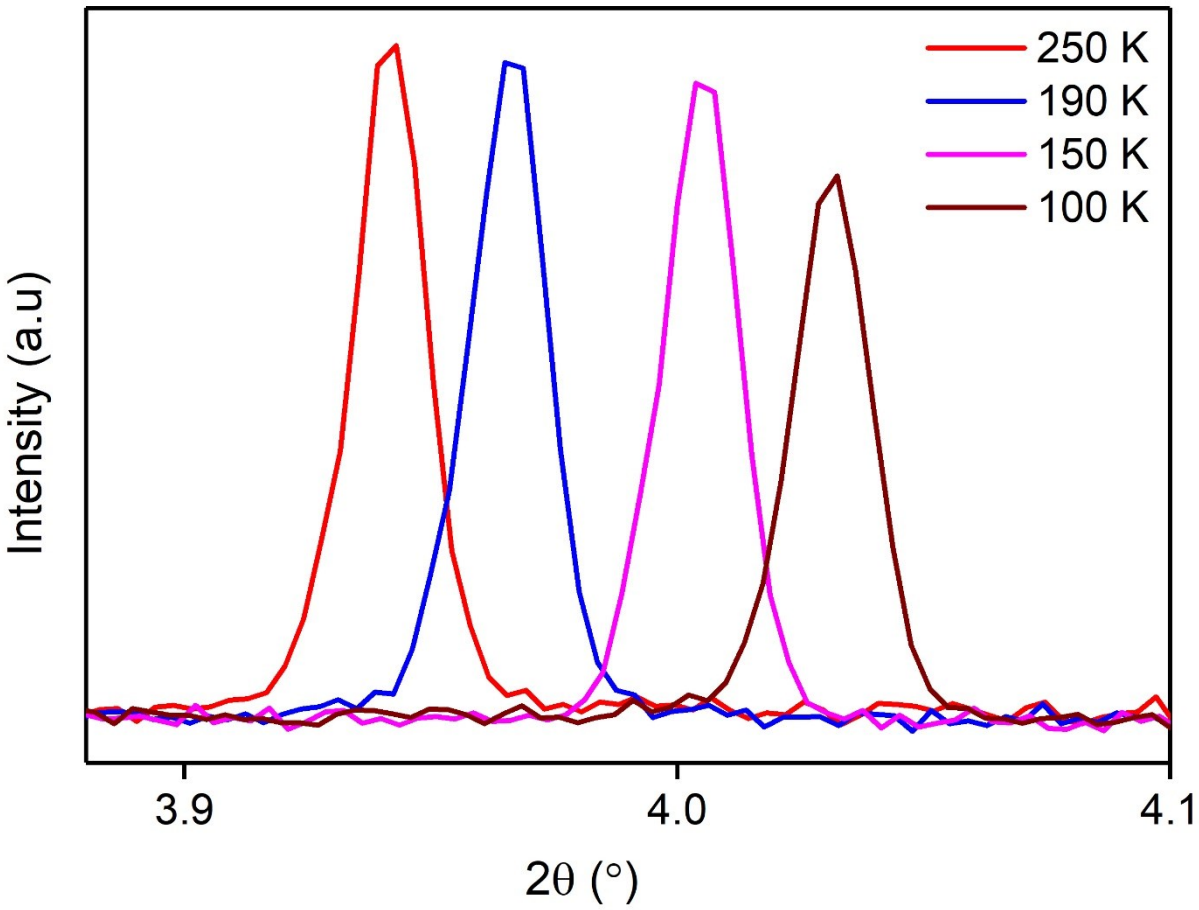

Figure S7. Comparison of the (110) reflection at the HS plateau (280 K, black), the ~$T_{½}$ (190 K, blue), the ~intermediate plateau (150 K, pink) and the LS plateau (100 K, brown).

S4. Single crystal X-ray diffraction

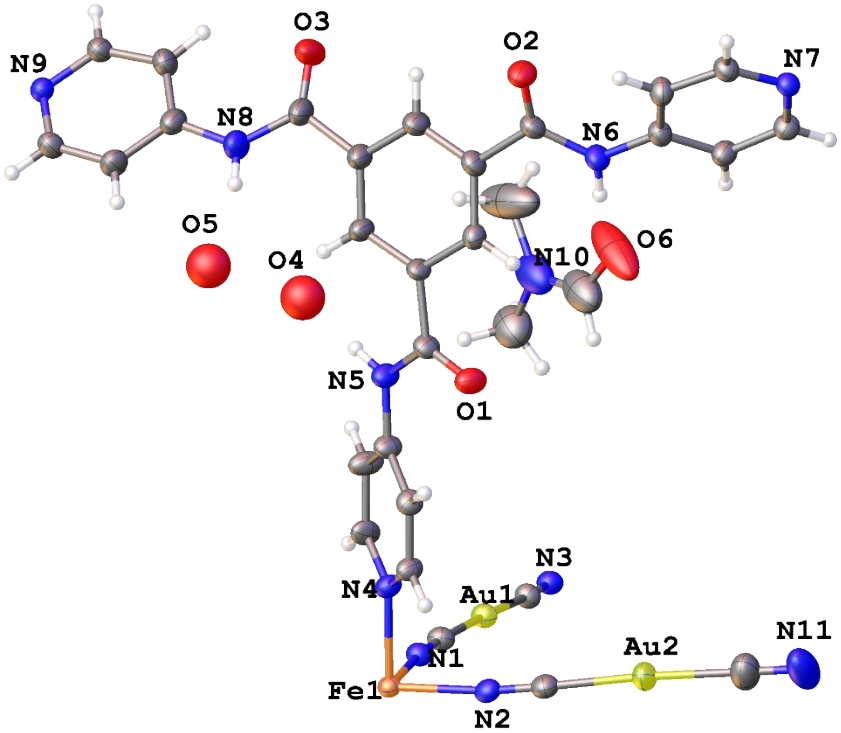

Figure S8. Asymmetric unit of $[Fe^{II}(Tbenpy)(Au(CN)_2)_2]\cdot\{2H_2O,DMF\}$ at 100 K

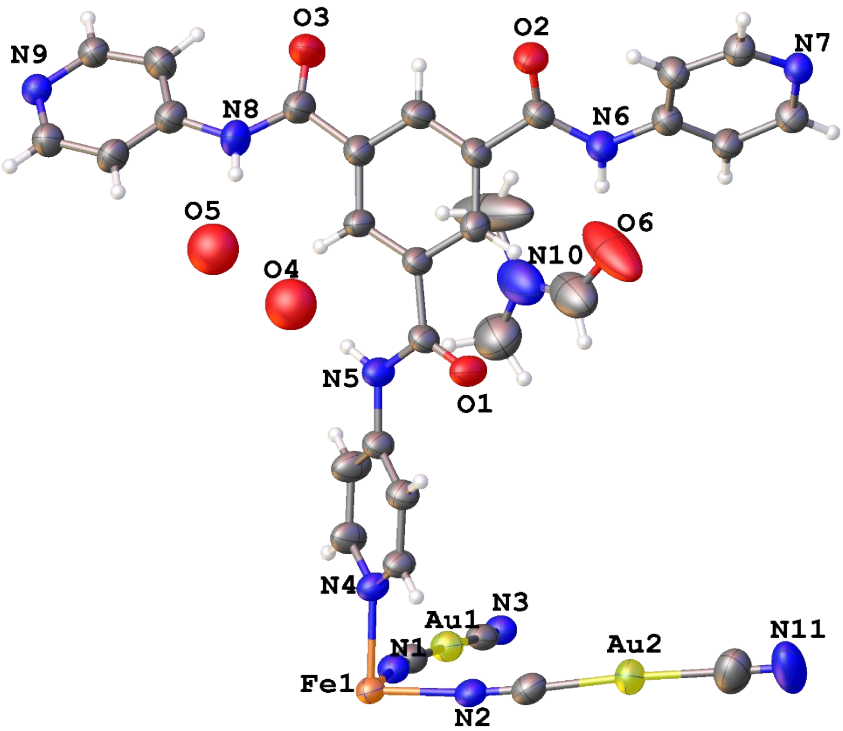

Figure S9. Asymmetric unit of $[Fe^{II}(Tbenpy)(Au(CN)_2)_2]\cdot\{2H_2O,DMF\}$ at 150 K

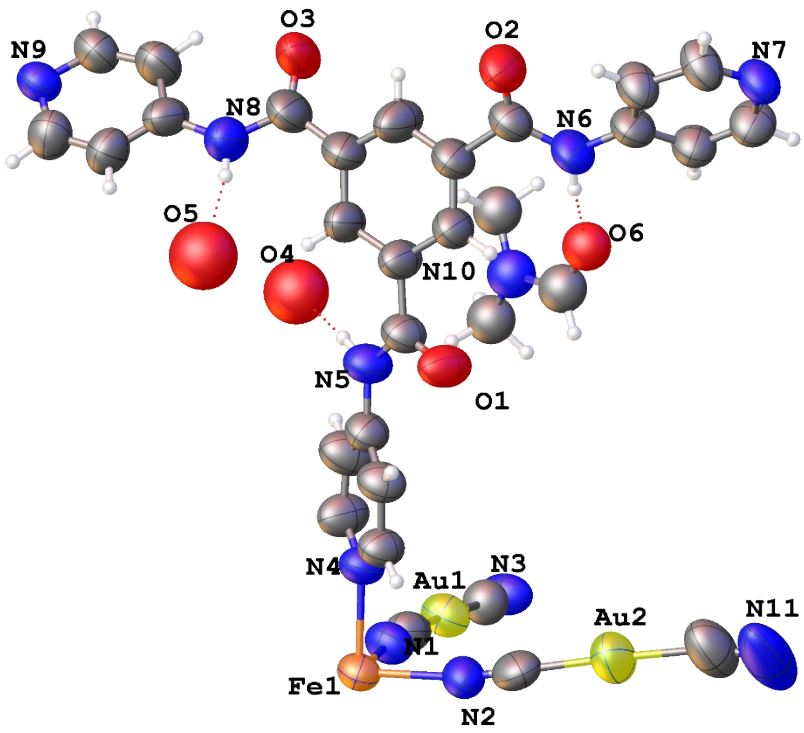

Figure S10.

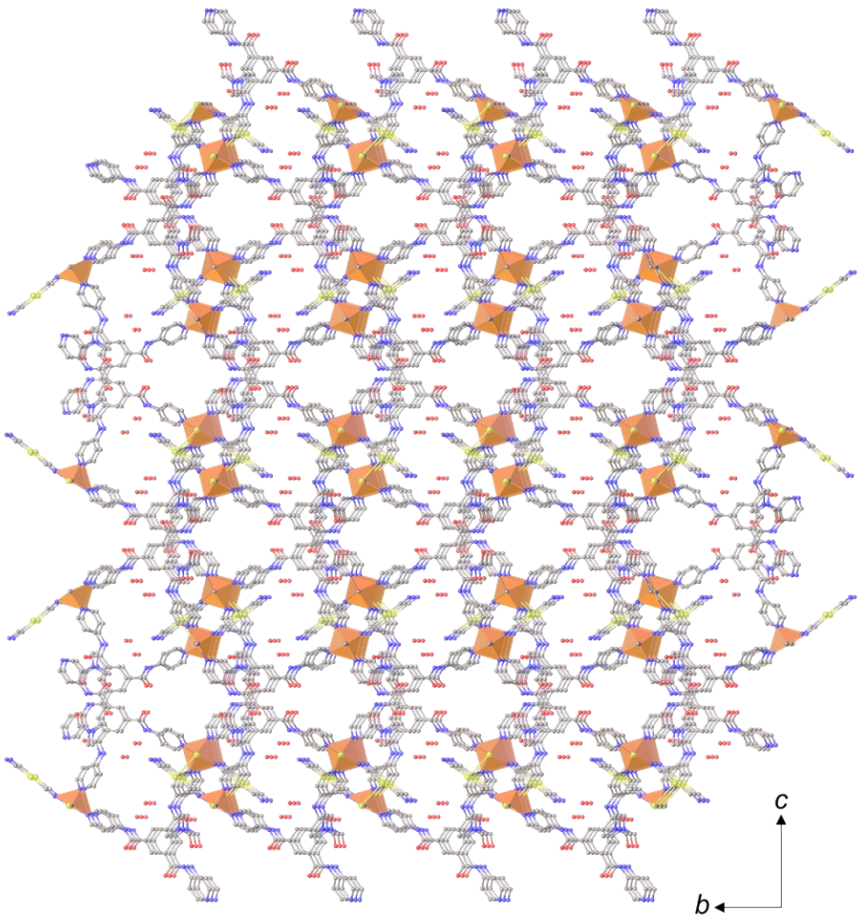

Asymmetric unit of $[Fe^{II}(Tbenpy)(Au(CN)_2)_2]\cdot\{2H_2O,DMF\}$ at 250 K

Figure S11. View of the $[Fe^{II}(Tbenpy)(Au(CN)_2)_2]\cdot\{2H_2O,DMF\}$ showing the water and DMF guest molecules in the pores. Hydrogen atoms are omitted for clarity.

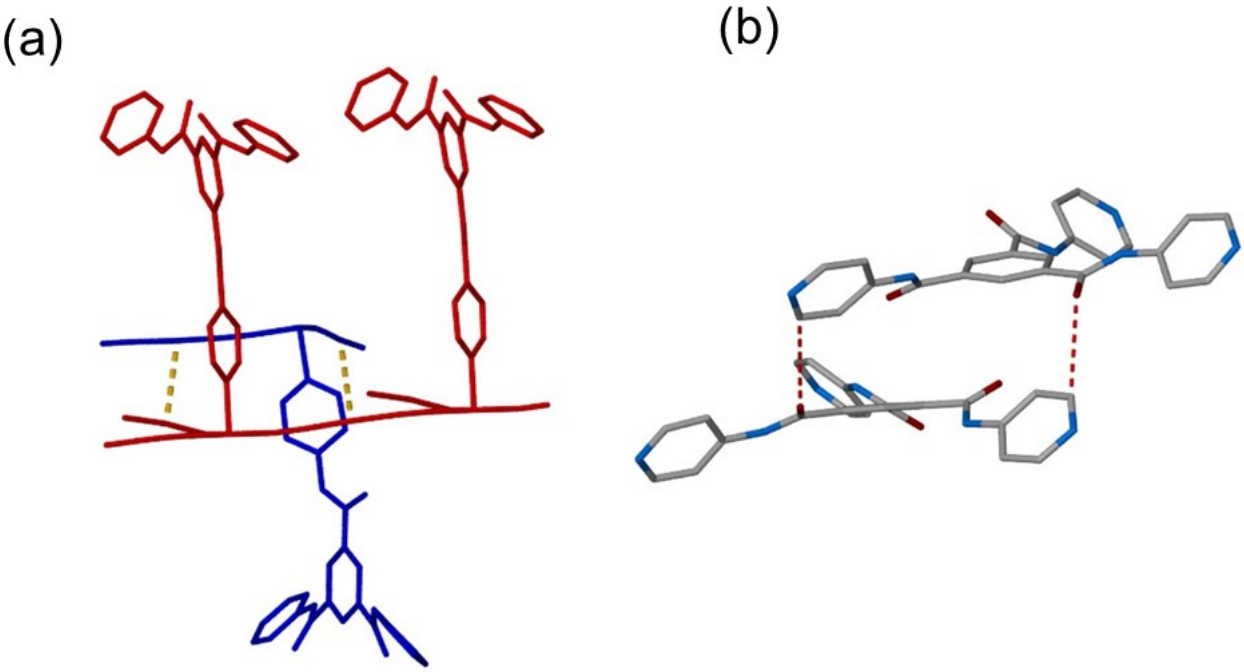

Figure S12. Structural representation of the (a) Au…Au interactions and (b) ligand – ligand interactions. Hydrogen atoms and guest molecules are omitted for clarity. See Table S2: Au…Au, CH…O.

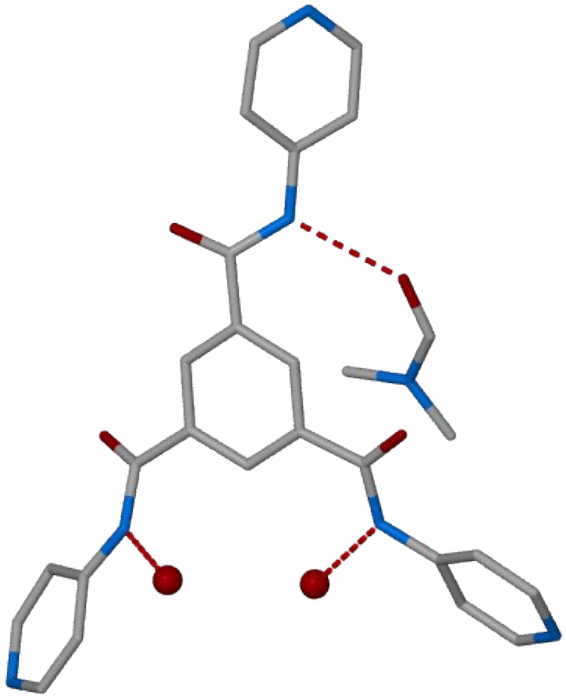

Figure S13. Structural representation of the host-guest hydrogen-bonding interactions involving the N(H) group of the Tbenpy ligand. Hydrogen atoms have been omitted for clarity. See Table S2: NH…H_2O, NH…DMF.

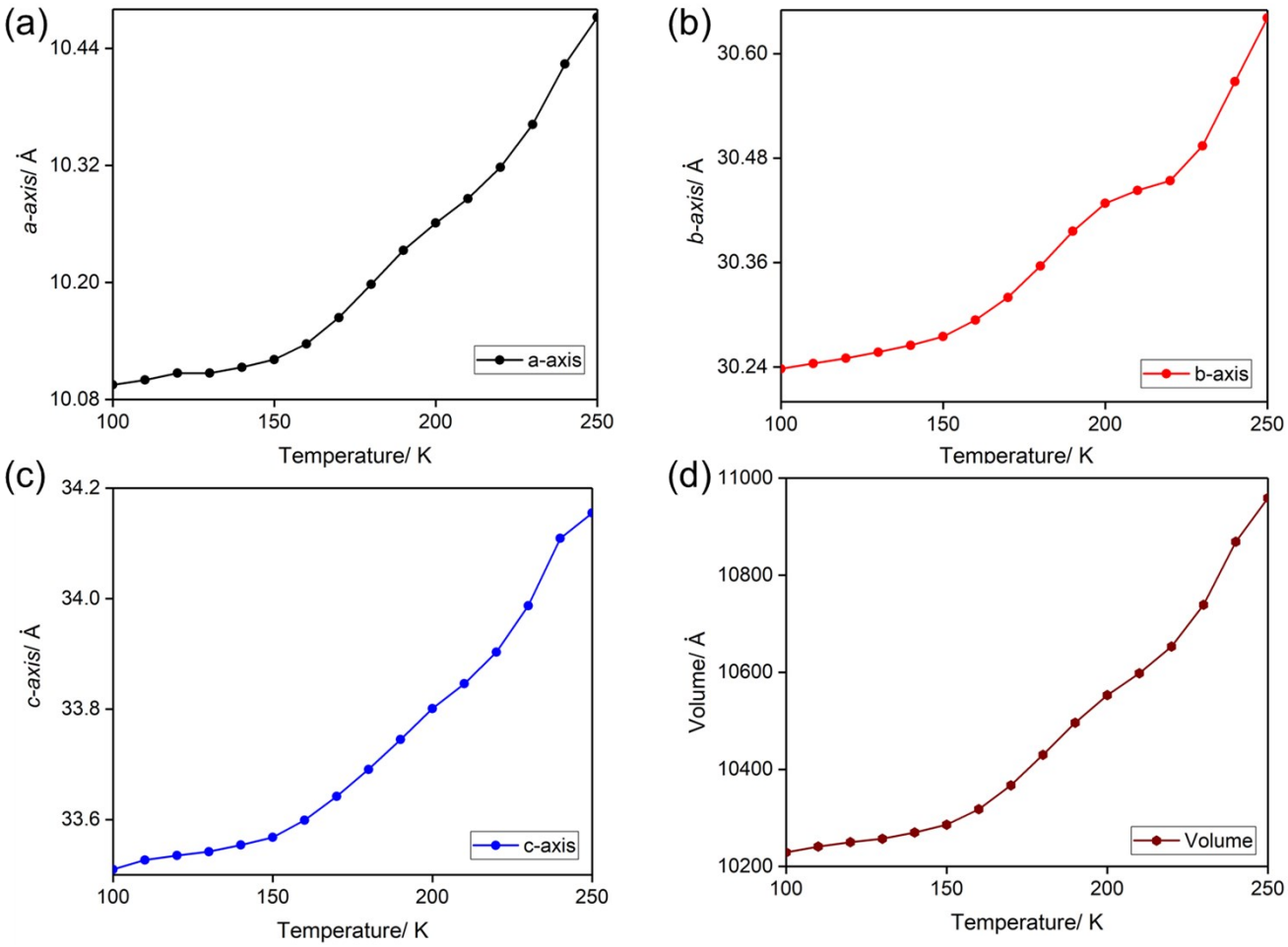

Figure S14. Plot of the (a) *a*-axis, (b) *b*-axis, (c) *c*-axis and (d) unit cell volume evolution versus temperature (100 -250 K) for $[Fe^{II}(Tbenpy)(Au(CN)_2)_2]\cdot\{2H_2O,DMF\}$ from single crystal data.

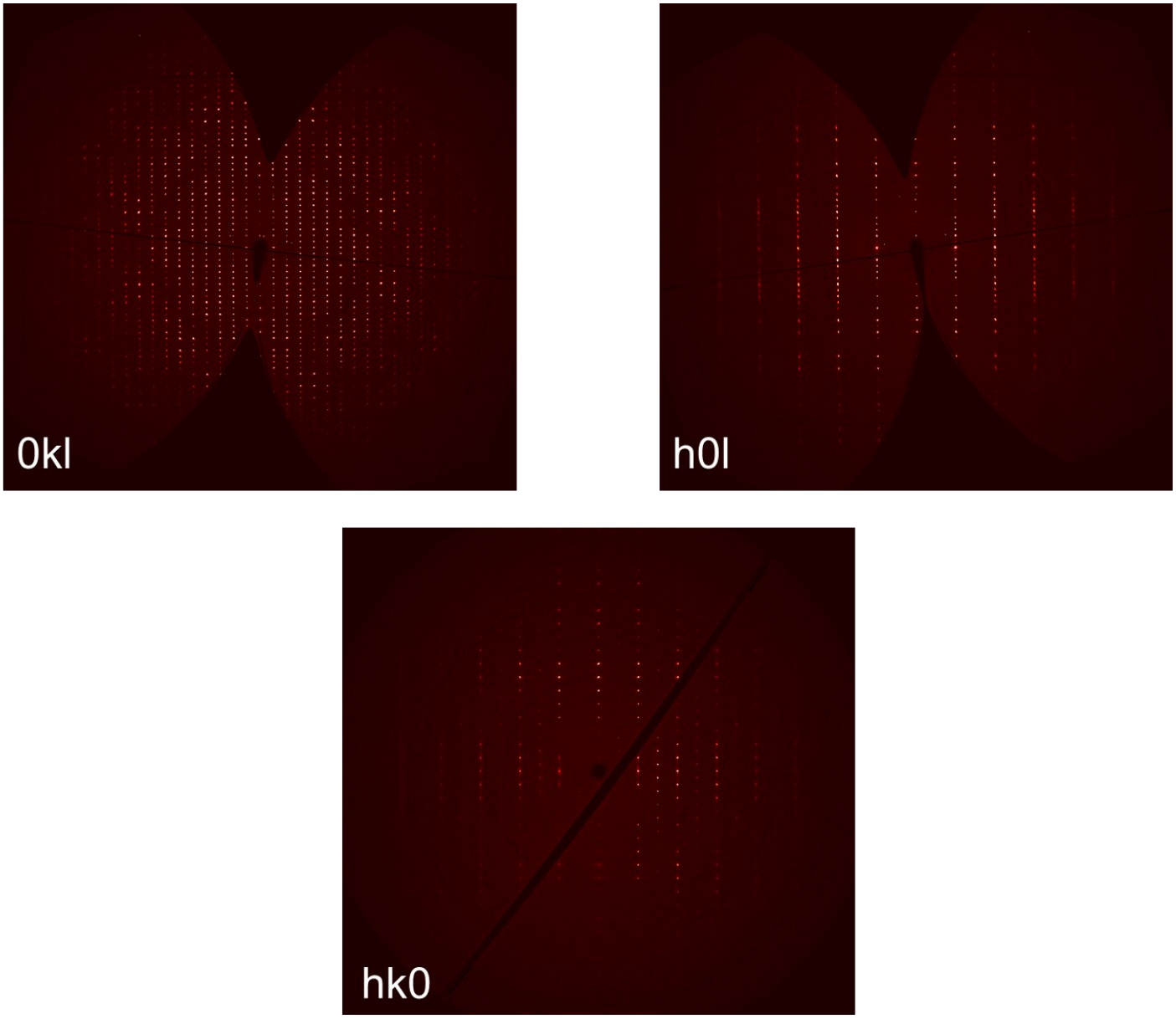

Figure S15. Precession images of $[Fe^{II}(Tbenpy)(Au(CN)_2)_2]\cdot\{2H_2O,DMF\}$ generated from the single crystal data at 250 K.

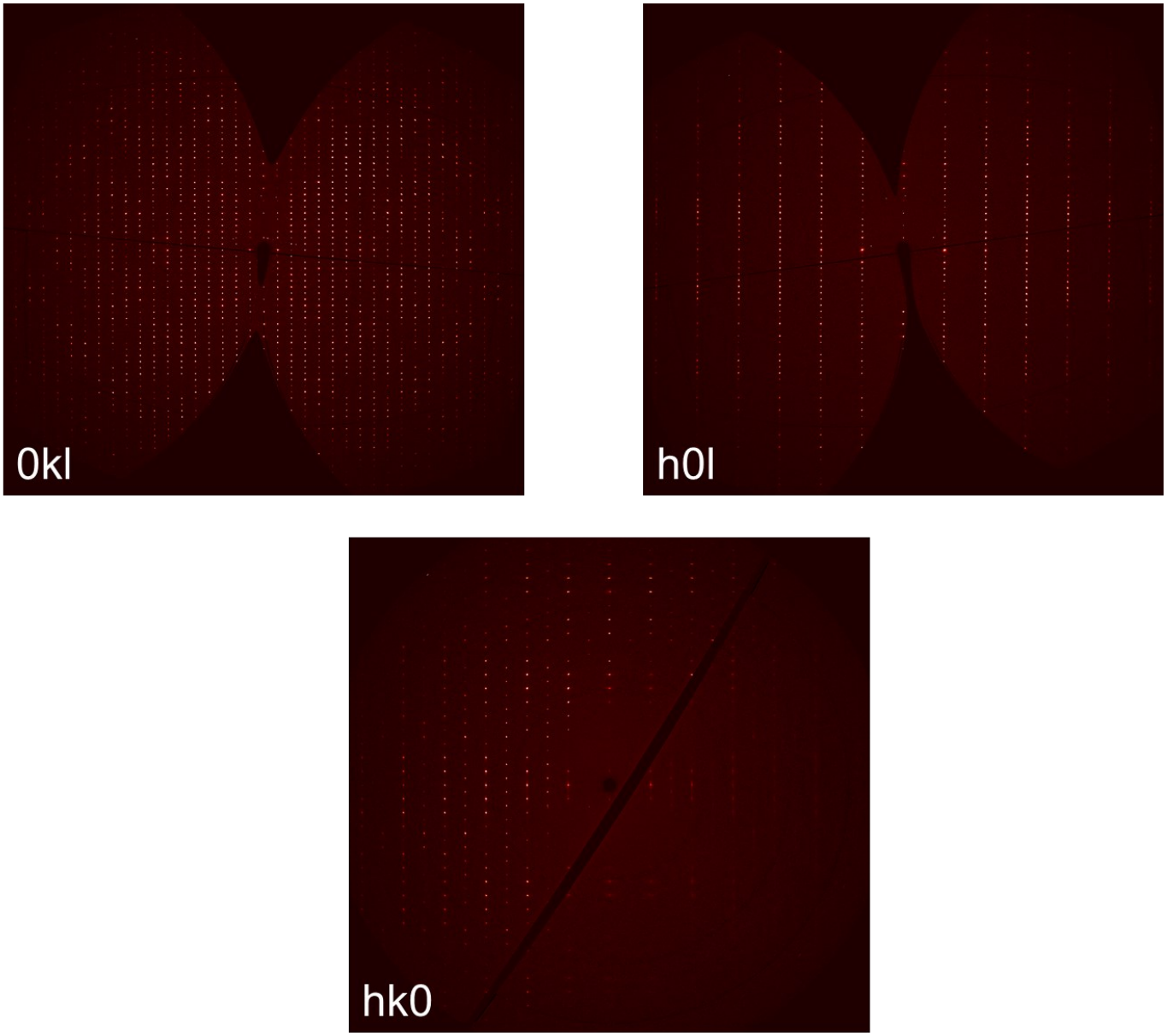

Figure S16. Precession images of $[Fe^{II}(Tbenpy)(Au(CN)_2)_2]\cdot\{2H_2O,DMF\}$ generated from the single crystal data at 150 K.

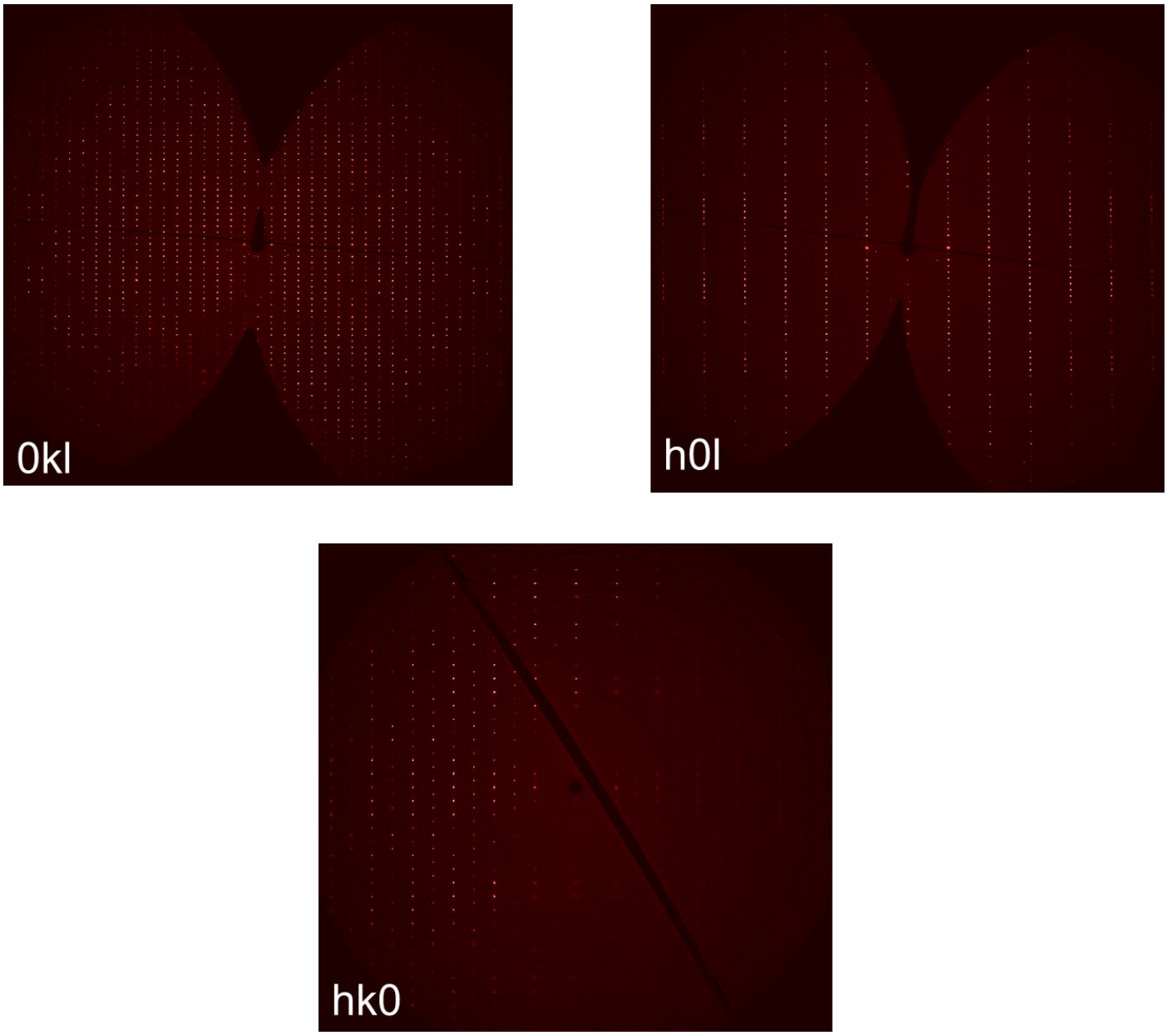

Figure S17. Precession images of $[Fe^{II}(Tbenpy)(Au(CN)_2)_2]\cdot\{2H_2O,DMF\}$ generated from the single crystal data at 100 K.

Table S1. Crystallographic data and refinement parameters

Parameters								
Empirical formula	$C_{31}H_{29}Au_2FeN_{11}O_6$							
Formula weight g/mol	1101.93							
T/K	250	240	230	220	210	200	190	180
Crystal system	Orthorhombic							
Space group	$C222_1$							
***a*/ Å**	10.472(2)	10.424(2)	10.362(2)	10.318(2)	10.286(2)	10.261(2)	10.233(2)	10.198(2)
***b*/ Å**	30.641(6)	30.568(6)	30.494(6)	30.455(6)	30.443(6)	30.428(6)	30.396(6)	30.356(6)
***c*/ Å**	34.155(7)	34.109(7)	33.987(7)	33.903(7)	33.846(7)	33.801(7)	33.745(7)	33.691(7)
Volume/ Å^3	10959(4)	10869(4)	10739(4)	10653(4)	10598(4)	10553(4)	10496(4)	10430(4)
ρ_{calc} g/cm^3	1.330	1.341	1.357	1.368	1.376	1.381	1.389	1.398
F(000)	4160							
μ / mm^{-1}	5.641	5.688	5.756	5.803	5.833	5.858	5.890	5.927
θ min-max/°	1.457 32.064	1.460 32.312	1.464 32.280	1.466 32.048	1.467 32.151	1.468 32.151	1.469 32.070	1.471 32.162
Crystal size	0.1 × 0.1 × 0.01							
Data/restraints/parameters	16062/ 0 /407	15941/ 0 /412	15763/ 0 /417	15275/ 0 /422	15527/ 0 /422	15464/ 0 /422	15332/ 0 /423	15248/ 0 /422
Goodness-of-fit on F^2	1.072	1.060	0.993	0.993	0.962	1.011	1.029	1.040
R_1 [$I > 2\sigma(I)$, all data] [a]	0.0951, 0.1233	0.1096, 0.1602	0.1024, 0.1523	0.0905, 0.1325	0.0785, 0.1002	0.0695, 0.0809	0.0619, 0.0666	0.0631, 0.0671
wR_2 [$I > 2\sigma(I)$, all data] [b]	0.2692, 0.3047	0.2972, 0.3481	0.2760, 0.3264	0.2589, 0.3112	0.2330, 0.2615	0.2064, 0.2228	0.1887, 0.1967	0.1918, 0.1991
Flack	0.379(4)	0.465(5)	0.438(6)	0.448(4)	0.439(3)	0.435(3)	0.517(2)	0.506(2)

Table S1 continued. Crystallographic data and refinement parameters

[a]R1 = ∑||Fo| − |Fc||/∑|Fo|. [b]wR2 = [∑w(Fo 2 − Fc 2)2 /∑w(Fo 2)2] ½

Parameters								
Empirical formula	$C_{31}H_{29}Au_2FeN_{11}O_6$							
Formula weight g/mol	1101.93							
T/K	170	160	150	140	130	120	110	100
Crystal system	Orthorhombic							
Space group	$C222_1$							
***a*/ Å**	10.164(2)	10.137(2)	10.121(2)	10.113(2)	10.107(2)	10.104(2)	10.100(2)	10.095(2)
***b*/ Å**	30.319(6)	30.295(6)	30.275(6)	30.265(6)	30.257(6)	30.250(6)	30.244(6)	30.238(6)
***c*/ Å**	33.642(7)	33.599(7)	33.568(7)	33.554(7)	33.542(7)	33.535(7)	33.527(7)	33.510(7)
Volume/ Å^3	10367(4)	10318(4)	10286(4)	10270(4)	10257(4)	10250(4)	10241(4)	10229(4)
ρ_{calc} g/cm^3	1.406	1.413	1.417	1.420	1.421	1.422	1.423	1.425
F(000)	4160							
μ / mm^{-1}	5.963	5.991	6.010	6.019	6.027	6.031	6.036	6.043
θ min-max/°	1.473 32.138	1.475 32.170	1.476 32.129	1.476 32.152	1.477 32.170	1.477 32.180	1.477 32.192	1.478 32.208
Crystal size	0.1 × 0.1 × 0.01							
Data/restraints/parameters	15188/ 0 /452	15123/ 0 /452	15045/ 0 /452	15005/ 0 /452	14964/ 0 /452	14944/ 0 /452	14933/ 0 /452	16062/ 0 /407
Goodness-of-fit on F^2	1.047	1.048	1.070	1.053	1.069	1.063	1.059	1.081
R_1 [$I > 2\sigma(I)$, all data] [a]	0.0639, 0.0675	0.0628, 0.0653	0.0581, 0.0594	0.0565, 0.0556	0.0541, 0.0548	0.0517, 0.0522	0.0494, 0.0496	0.0465, 0.0467
wR_2 [$I > 2\sigma(I)$, all data] [b]	0.1911, 0.1966	0.1861, 0.1901	0.1755, 0.1775	0.1676, 0.1689	0.1644, 0.1654	0.1550, 0.1558	0.1481, 0.1484	0.1407, 0.1409
Flack	0.490(2)	0.482(2)	0.4707(19)	0.4588(18)	0.4510(17)	0.4406(16)	0.4334(16)	0.4153(16)

Table S2. Selected structure parameters and hydrogen bonding for $[Fe^{II}(Tbenpy)(Au(CN)_2)_2]\cdot\{2H_2O,DMF\}$

Selected parameters	**Temperature**								
	250	240	230	220	210	200	190	180	170
$d_{<Fe-N>}$ /Å [a]	2.166(13)	2.151(15)	2.131(12)	2.080(13)	2.073(12)	2.060(10)	2.039(9)	2.022(9)	2.005(8)
Fe1 C≡N /°	169.4-174.6	171.5-174.4	169-174.9	169.9-174.4	170.9-175.3	171.5-174.7	171.4-175.0	171.2-175.6	172.3-174.7
Σ^{Fe1} /° [b]	16.5	19	19.9	15.5	12.3	15.3	15.8	15.4	16.0
Fe1-N-N^{py} /°	89.8	89.8	88.8	89.1	90.0	89.6	89.3	89.9	89.8
Host···host Interactions/ Å									
O1···C28	3.140	3.170	3.140	3.110	3.120	3.140	3.142	3.155	3.143
Au···Au	3.279	3.261	3.252	3.246	3.246	3.245	3.248	3.243	3.238
Guest···host Interactions/ Å									
O4W···N5	2.940	2.950	2.890	2.980	2.900	2.930	2.980	2.960	2.980
O5W··· N8	2.900	2.800	2.820	2.860	2.880	2.940	2.920	2.930	2.910
O5W···N11	2.940	2.800	2.930	3.080	3.000	2.950	2.910	2.890	2.900
O6··· N6	2.890	2.890	2.860	2.920	2.859	2.859	2.862	2.859	2.845

Table S2 continued. Selected structure parameters and hydrogen bonding for $[Fe^{II}(Tbenpy)(Au(CN)_2)_2]\cdot\{2H_2O,DMF\}$

[a]Average bond length of the Fe^{II} octahedron

Selected parameters	**Temperature**						
	160	150	140	130	120	110	100
$d_{<Fe-N>}$ **/Å** [a]	1.989(8)	1.985(8)	1.983(8)	1.981(7)	1.979(7)	1.979(7)	1.975(7)
Fe1 C≡N /°	171.8-175.1	172.3-175.0	171.9-175.6	171.6-175.1	172.2-175.2	172.4-174.9	172.6-174.8
Σ^{Fe1} **/°** [b]	16.4	15.7	16.2	15.9	15.3	14.7	14.6
Fe1-N-N^{py} /°	90.2	90.3	90.2	90.1	90.3	90.1	90.3
***Host···host Interactions/* Å**							
O1···C28	3.139	3.137	3.142	3.142	3.141	3.145	3.148
Au···Au	3.235	3.232	3.231	3.230	3.227	3.228	3.227
***Guest···host Interactions/* Å**							
O4W···N5	2.970	2.970	2.980	2.960	2.970	2.970	2.960
O5W··· N8	2.940	2.900	2.910	2.900	2.900	2.903	2.894
O5W···N11	2.920	2.920	2.900	2.910	2.900	2.890	2.880
O6··· N6	2.846	2.842	2.838	2.835	2.893	2.848	2.834

[b]Octahedral distortion parameter (sum of | 90 – θ | for the 12 cis angles of the Fe^{II} octahedron

S5. Magnetic susceptibility measurements

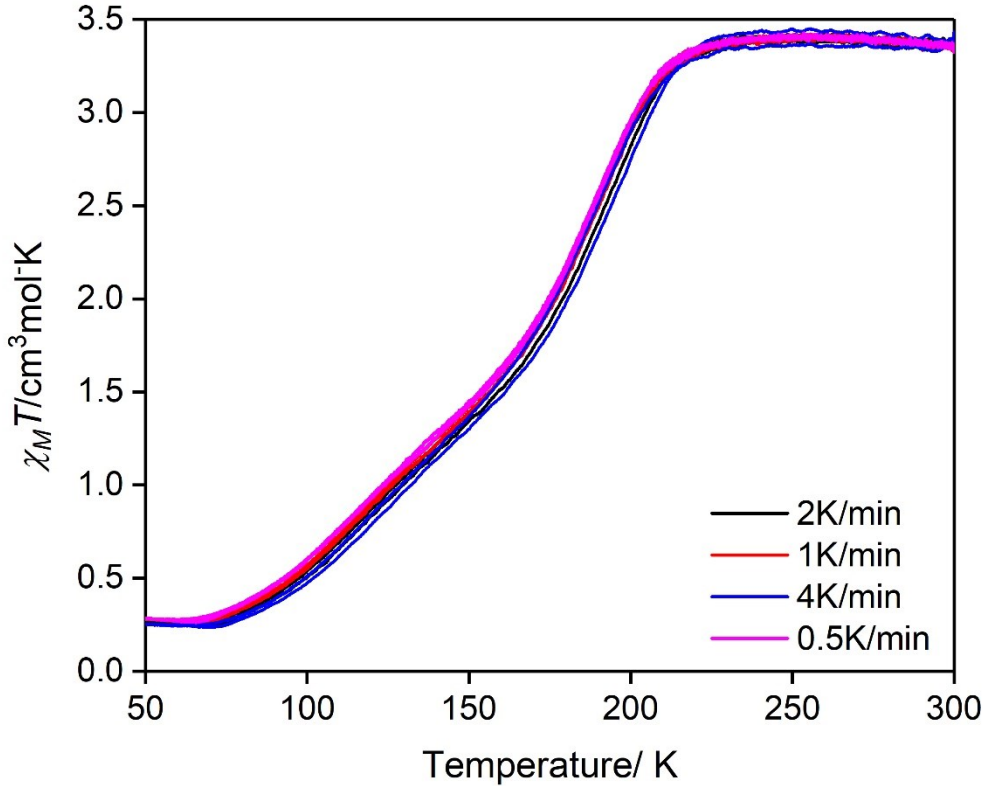

Figure S18. Variable scan rate magnetic susceptibility of $[Fe^{II}(Tbenpy)(Au(CN)_2)_2]\cdot\{2H_2O,DMF\}$ (2, 1, 4 and 0.5 K/min).

S6. Raman spectroscopy

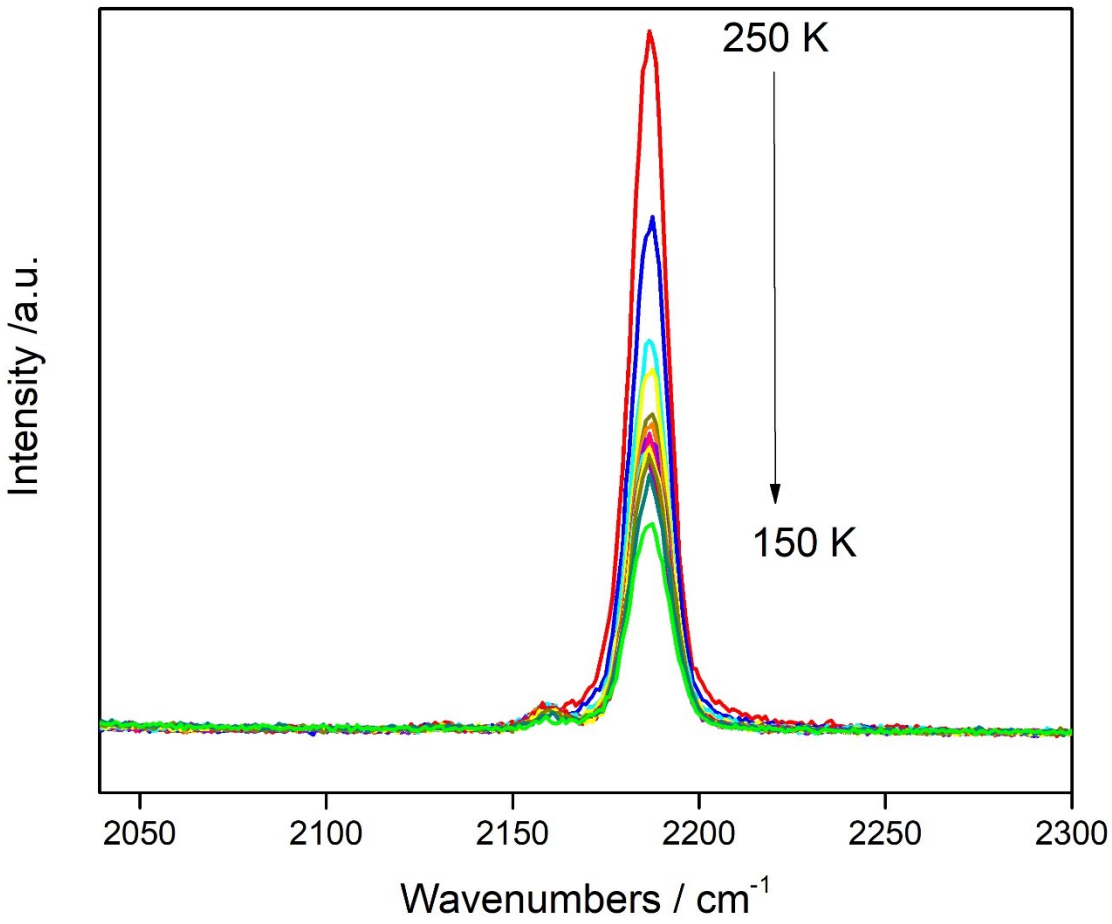

Figure S19. Variable temperature (250 – 150 K) Raman spectra comparison of the C-N stretching mode of the $Au(CN)_2$ units.

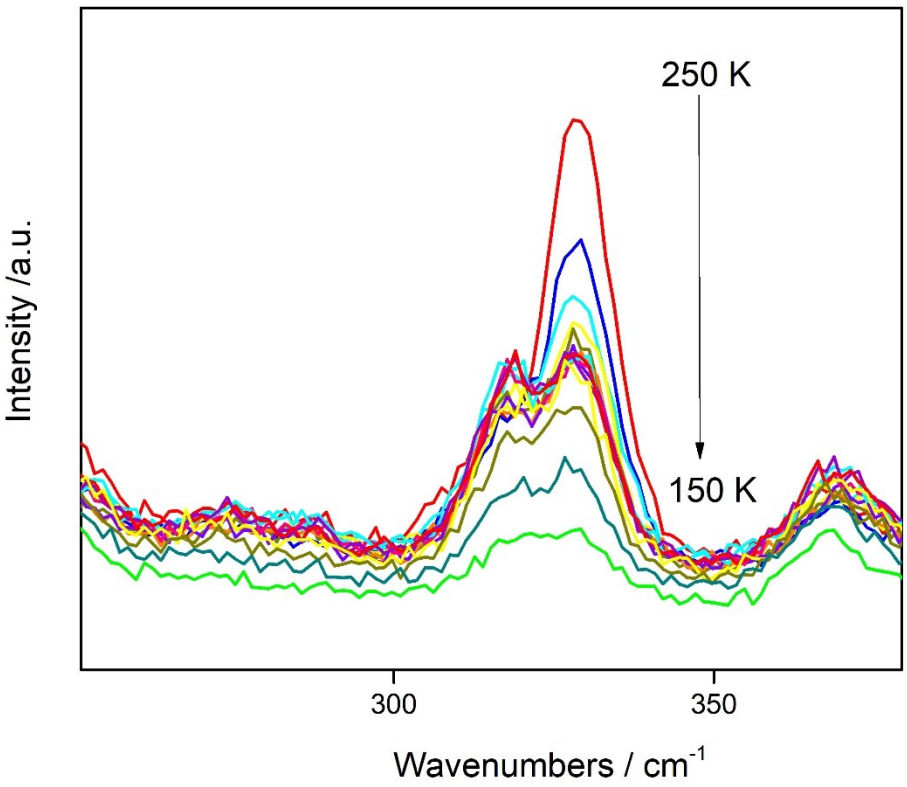

Figure S20. Variable temperature (250 - 150 K) Raman spectra comparison of the FeN_6 coordination sphere.

S7. References

1. S. Hong, Y. Zou, D. Moon and M. S. Lah, *Chemical communications*, 2007, 1707-1709.
2. D. Aragao, J. Aishima, H. Cherukuvada, R. Clarken, M. Clift, N. P. Cowieson, D. J. Ericsson, C. L. Gee, S. Macedo and N. Mudie, *Journal of synchrotron radiation*, 2018, **25**, 885-891.
3. T. M. McPhillips, S. E. McPhillips, H.-J. Chiu, A. E. Cohen, A. M. Deacon, P. J. Ellis, E. Garman, A. Gonzalez, N. K. Sauter and R. P. Phizackerley, *Journal of synchrotron radiation*, 2002, **9**, 401-406.
4. W. Kabsch, *Journal of applied crystallography*, 1993, **26**, 795-800.
5. Bruker, v2018.1, Bruker AXS Inc., Madison, Wisconsin, USA, 2018.
6. G. M. Sheldrick, *Acta Crystallographica Section A: Foundations and Advances*, 2015, **71**, 3-8.
7. G. M. Sheldrick, *Acta Crystallographica Section C: Structural Chemistry*, 2015, **71**, 3-8.
8. O. V. Dolomanov, L. J. Bourhis, R. J. Gildea, J. A. Howard and H. Puschmann, *Journal of applied crystallography*, 2009, **42**, 339-341.
9. L. J. Barbour, A software tool for supramolecular crystallography. Elsevier: 2001.
10. K. S. Wallwork, B. J. Kennedy and D. Wang, In *AIP Conference Proceedings*, *American Institute of Physics,* 2007, **879**, 879-882.
11. B. Schmitt, C. Brönnimann, E. Eikenberry, F. Gozzo, C. Hörmann, R. Horisberger and B. Patterson, *Nuclear Instruments and Methods in Physics Research Section A: Accelerators, Spectrometers, Detectors and Associated Equipment*, 2003, **501**, 267-272.
12. A. A. Coelho, *Journal of Applied Crystallography*, 2018, **51**, 210-218.